DIFFUSE-REFLECTANCE OF OCEANIC SHALLOW WATERS - INFLUENCE OF WATER DEPTH AND BOTTOM ALBEDO

S Maritorena, A Morel, B Gentili

Limnol. Oceanogr., 39(7), 1994, 1689–1703

Diffuse reflectance of oceanic shallow waters: Influence of water depth and bottom albedo

Stéphane Maritorena
Laboratoire d'Ecologie Marine, Université Française du Pacifique, BP 6570—Faaa/Aéroport, Tahiti, French Polynesia

André Morel and Bernard Gentili
Laboratoire de Physique et Chimie Marines, Université Pierre et Marie Curie et CNRS, BP 8, 06230 Villefranche-sur-Mer, France

Abstract

We used simplifying assumptions to derive analytical formulae expressing the reflectance of shallow waters as a function of observation depth and of bottom depth and albedo. These formulae also involve two apparent optical properties of the water body: a mean diffuse attenuation coefficient and a hypothetical reflectance which would be observed if the bottom was infinitely deep. The validity of these approximate formulae was tested by comparing their outputs with accurate solutions of the radiative transfer obtained under the same boundary conditions by Monte Carlo simulations. These approximations were also checked by comparing the reflectance spectra for varying bottom depths and compositions determined in coastal lagoons with those predicted by the formulae. These predictions were based on separate determinations of the spectral albedos of typical materials covering the floor, such as coral sand and various green or brown algae. The simple analytical expressions are accurate enough for most practical applications and also allow quantitative discussion of the limitations of remote-sensing techniques for bottom recognition and bathymetry.

As early as 1944, Duntley used a spectrograph mounted in a glass-bottomed boat or flown in an airplane to analyze radiances emerging from the ocean and shallow waters. He evidenced the influence of the water depth on the spectral composition of the upward flux (Duntley 1963). Using a Monte Carlo technique, Plass and Kattawar (1972) calculated the radiative field in the atmosphere–ocean system and in particular examined the dependence of the upward flux on the albedo of the ocean floor. Gordon and Brown (1974) studied the diffuse reflectance of a shallow ocean using Monte Carlo simulations and a probabilistic approach. Gordon and Brown provided an analysis based on photon history of the light field as modified by the presence of a reflecting bottom. In addition, Ackleson and Klemas (1986) developed a two-flow model that simulated the light field within a canopy of bottom-adhering plants. A single scattering approximation for irradiance reflectance was also designed for optically shallow waters (Philpot 1987); this model was thereafter used to explore the feasibility of mapping bathymetry with remote-sensing techniques (Philpot 1989).

In the hope that bathymetric and bottom recognition surveys could be made from air- or satellite-borne sensors, several approximate solutions have been proposed for interpreting radiometric signals over shallow waters. These solutions led to the development of various empirical algorithms (e.g. *see* Lyzenga 1978, 1981; Paredes and Spero 1983; Clark et al. 1987) that could be used in problems in which the number of unknowns typically exceeds the number of equations (Philpot 1989). The inherent optical properties of the water, the water depth, and the bottom type are the main physical agents governing the magnitude and spectral composition of the backscattered flux. The radiance distribution incident on the surface, related to sun position and sea state, are also involved, but with a lesser influence.

With modern computers and appropriate numerical techniques, "exact" solutions of the radiative transfer equation (RTE) are now derivable (Mobley et al. 1994). However, such computations, made case-by-case, deal with specified water properties and boundary conditions. An analytical formulation able to con-

Aknowledgments

We thank C. E. Payri for help and advice during the experimental phase of this study, in particular when we were sampling and identifying the algae. We are indebted to J. T. O. Kirk for comments and suggestions on an earlier version, resulting in an improved theoretical analysis. We also thank two anonymous reviewers for criticism.

Notation

a	Absorption coefficient, m^{-1}
b	Scattering coefficient, m^{-1}
b_{bd}	Diffuse backscattering coefficient for downwelling light stream, m^{-1}
c	Attenuation coefficient ($c = a + b$), m^{-1}
ω	Single scattering albedo ($= b/c$)
η	Ratio of molecular scattering to total scattering
Z	Depth measured from the surface downward, m
H	Bottom depth, m
τ	Optical depth ($= cZ$)
E_d, E_u	Downward and upward irradiance, W m^{-2}
R	Reflectance or irradiance ratio ($=E_u : E_d$)
R_∞	Reflectance of the infinitely deep ocean
B, C	Bottom and column (used as subscripts)
A	Bottom albedo
K_d	Vertical attenuation for downwelling irradiance, m^{-1}
κ	Vertical attenuation coefficient of the flux scattered upward from a thin layer of water, m^{-1}
μ_d	Average cosine of the zenith angle of downwelling photons
μ_u	Average cosine of the nadir angle of upwelling photons
θ_0	Solar zenith angle
λ	Wavelength, nm

tinuously account for the interwoven influences of the three agents mentioned above would be of more extended use and general application. Because there is no analytical solution of the RTE, any analytical expression remains inevitably approximate. Therefore, the safe use of such expressions requires that the underlying approximations are acceptable and their impact quantified.

In this paper, we use an approach derived from the two-flow equations to obtain approximate formulae based on a set of simplifying assumptions. These equations describe the upwelling irradiance and the irradiance ratio (or reflectance) inside a water body, between the bottom (with a given albedo) and the top layer. Our aim is to assess the validity of such approximate solutions of the RTE. The validation is made in two distinct ways. First, the approximate solutions are compared to exact solutions of the RTE obtained via Monte Carlo simulations. Second, the spectral values of the reflectance in the presence of varying bottoms (composition and depth), as predicted from the approximate formulae, are compared to field data obtained in lagoonal waters of French Polynesia.

Theoretical background

In shallow waters, the upwelling irradiance just below the surface, $E_u(0)$, results from adding the flux backscattered by the water column (as if the bottom were black) and the flux reflected by the bottom (when it is not black) and then transmitted through the column, so that

$$E_u(0) = [E_u(0)]_C + [E_u(0)]_B. \quad (1)$$

The subscripts C and B stand for column and bottom (a list of notation is provided). The first term corresponds to the photons that have never interacted with the bottom, whereas those that have interacted with the bottom at least once form the second term. The wavelength is fixed, even if the adjective spectral and argument λ are omitted for brevity in the following equations.

To estimate the first term, consider an infinitely thin layer of thickness dZ at depth Z. At this level, the downwelling irradiance is $E_d(Z)$. The backscattering coefficient (or reflectance function) for the downwelling light stream (a hybrid property of the water medium, sensu Preisendorfer 1961) is denoted b_{bd}; the fraction of upwelling irradiance created by this layer is

$$dE_u(Z) = b_{bd}E_d(Z)\,dZ. \quad (2)$$

$E_d(Z)$ can be expressed as

$$E_d(Z) = E_d(0)\exp(-K_dZ).$$

$E_d(0)$ is the downwelling irradiance at null depth, and K_d is the diffuse attenuation for downwelling irradiance. Before it reaches the surface, $dE_u(Z)$ suffers an attenuation along the path from Z up to 0, expressed by $\exp(-\kappa Z)$, where κ is the vertical diffuse attenuation coefficient for upward flux as defined by Kirk (1989) and also introduced by Philpot (1987) with the symbol k'. This coefficient refers to an exponential attenuation (with distance traveled upward) of the upward flux originating from any thin layer. The contribution of the considered layer to the upwelling irradiance just below the surface is denoted $dE_u(Z \rightarrow 0)$; this term is expressed as

$$dE_u(Z \rightarrow 0) = b_{bd}E_d(0)\exp[-(K_d + \kappa)Z]\,dZ. \quad (3)$$

At this stage, the approximation (discussed later) consists of considering that b_{bd}, K_d, and

κ are not depth-dependent. Under such an assumption, the contributions of each layer between Z and 0 in forming $E_u(0, Z)$ can be summed, so that

$$E_u(0, Z) = b_{bd}E_d(0) \times \int_0^Z \exp[-(K_d + \kappa)Z]\, dZ$$
$$= (K_d + \kappa)^{-1} b_{bd}E_d(0) \times \{1 - \exp[-(K_d + \kappa)Z]\}. \quad (4)$$

For an infinite water depth ($Z = \infty$), Eq. 4 reduces to

$$E_u(0, \infty) = (K_d + \kappa)^{-1} b_{bd}E_d(0) = R(0, \infty)E_d(0). \quad (5)$$

$R(0, \infty) = (K_d + \kappa)^{-1} b_{bd}$ represents the reflectance at null depth of the deep ocean, hereafter denoted R_∞. For a column limited by the presence of a (perfectly absorbing) bottom at a depth H, Eq. 4 reads

$$E_u(0, H) = R_\infty E_d(0)\{1 - \exp[-(K_d + \kappa)H]\} = [E_u(0)]_C \quad (6)$$

and thus provides the first term in Eq. 1.

If the bottom is a Lambertian reflector with an albedo A, the reflected flux at level H (i.e. immediately above the bottom) is

$$[E_u(H)]_B = A\, E_d(H) = A\, E_d(0) \exp(-K_d H).$$

This contribution of the bottom to the upwelling irradiance will be attenuated from H up to the surface. If we suppose that this upward flux is attenuated with the same κ as above, the contribution of the bottom to the upward irradiance reaching the surface becomes

$$[E_u(0)]_B = A\, E_d(0)\exp(-K_d + \kappa)H]. \quad (7)$$

By adding Eq. 6 and 7, according to Eq. 1 we obtain

$$E_u(0) = E_d(0)\langle R_\infty\{1 - \exp[-(K_d + \kappa)H]\} + A \exp[-(K_d + \kappa)H]\rangle. \quad (8a)$$

Dividing by $E_d(0)$ and rearranging, the reflectance, $R(0, H)$, below the surface of a homogeneous ocean bounded below by a reflecting bottom at depth H, is

$$R(0, H) = R_\infty + (A - R_\infty)\exp[-(K_d + \kappa)H]. \quad (8b)$$

This expression is identical to that of Philpot (equation 38, 1987; equation 4, 1989). To the extent that the two kinds of upward fluxes, either scattered by the series of thin layers or reflected by the bottom, do not have the same geometrical structure, they are not attenuated in the same way. If κ_C and κ_B denote the attenuation coefficients for the upward streams originating from the water column and from the bottom, Eq. 8b must be written as

$$R(0, H) = R_\infty + \exp(-K_d H) \times [A \exp(-\kappa_B H) - R_\infty \exp(-\kappa_C H)]. \quad (8c)$$

Derivation of the approximate solution

The approximate character of the above equations (including Eq. 8c) results from the supposed invariability with respect to depth of b_{bd}, K_d, κ_C, and κ_B which has allowed simple integrations to be performed. Because they depend on progressive rearrangement of the radiative field, all of these coefficients cannot be constant, even for a homogeneous water body. Near the surface, K_d and b_{bd} depend on the illumination conditions prevailing above, whereas κ_C and κ_B depend on the distance traveled upward. Among the three attenuation coefficients involved in Eq. 8c, there are notable differences.

Because of the horizontally biased angular distribution of the photons backscattered by a thin layer, the corresponding upward stream is attenuated more rapidly than the downwelling flux; therefore κ_C is always greater than K_d (Kirk 1989), even if κ_C decreases when the distance traveled from the thin layer of origin is increasing. For instance, Kirk (1989) showed that at mideuphotic depth, κ_C would be ~ 2.5 K_d when K_d takes its minimal value, i.e. when there is no sky radiation and the sun is vertical (Kirk 1984). Within the frame of the two-flow approach, the ratio of κ_C to K_d is essentially governed by the ratio of μ_d to μ_u, the average cosines for downwelling and upwelling irradiance. Therefore, $\kappa_C : K_d$ decreases as scattering becomes relatively more important than absorption because in a more diffuse regime μ_d decreases, while μ_u remains about the same (*see* Philpot 1989).

The situation is different for κ_B. With a bottom acting as a lambertian reflector, the angular distribution of reflected photons (mean cosine, 0.5) is much less oblique than for backscattered photons so that the corresponding upward flux is less attenuated along its vertical journey. Very close to the bottom, κ_B could be as high as $2K_d$ if K_d is minimum (i.e. when K_d is equal to the absorption coefficient—a situation that would occur in a purely absorbing medium and when the incident light is vertical). In natural conditions, κ_B, appropriate for a finite distance H, is $<2K_d$ (and always $<\kappa_C$). In the presence of a detectable bottom, the respective roles of K_d and κ_C are determined by the respective values of A and R_∞. With A supposedly larger than R_∞, the first term in parentheses in Eq. 8c is preponderant and thus reinforces the influence of the smallest coefficient κ_B compared to that of κ_C, which applies only on R_∞. This conclusion must be reversed if the "bottom contrast" is negative, when $(A - R_\infty) < 0$.

The approximate solution assumes that the three attenuation coefficients can be replaced by an operational and unique K coefficient, so that Eq. 8c becomes

$$R(0, H) = R_\infty + (A - R_\infty)\exp(-2KH). \quad (9a)$$

This simplification is necessary because, in contrast with K_d (easily determined or guessed), the κ values are not directly measurable and have specific values for each situation and geometry. In practice, K_d will be used later to quantify an operational K. The use of $2K_d$ for the exponential decay, however, will lead to an underestimate of the actual attenuation suffered by the albedo difference, $(A - R_\infty)$. As a consequence, Eq. 9a will incorrectly estimate the reflectances $R(0, H)$ to an extent that remains unquantified. Note that Eq. 9a is referred to by O'Neill and Miller (1989) as the "most-familiar form" of the shallow-water reflectance model, with no indication of the inherent approximations and expected deviations. This equation is a particular solution of the general equation, derived under the same assumption (a unique K coefficient), that provides R at any depth Z (with $0 < Z < H$):

$$R(Z, H) = R_\infty + (A - R_\infty)\exp[-2K(H - Z)]. \quad (9b)$$

Equations 9a and b show that the reflectance of a water column limited by a reflecting bottom is equal to the reflectance of the same water body in absence of a bottom (R_∞) plus the bottom contrast ($A - R_\infty$) (positive or negative) after this contrast has been modulated by the depth of the bottom through the exponential attenuation, $\exp[-2K(H - Z)]$.

By constraining $R(0, H)$ to be constant in Eq. 9a regardless of the bottom depth and then differentiating, we obtain

$$dH = (2K)^{-1}\,[dA/(A - R_\infty)], \quad (10a)$$

or for finite differences

$$(H_1 - H_2) = (2K)^{-1}\ln[(A_1 - R_\infty) \div (A_2 - R_\infty)]. \quad (10b)$$

These expressions show how the depth and bottom albedo must be related to produce the same reflectance at the surface. For a given water and a constant K value, a change in depth proportional to the relative change in albedo would leave the reflectance unchanged (Eq. 10a). According to Eq. 10b, a bottom at depth H_1 with an albedo A_1 produces, just below the surface, the same signal as another bottom at H_2 with A_2. As a consequence, if the optical properties of the water body (R_∞ and K) are known, the increase in reflectance due to the presence of a bottom can be interpreted in terms of depth only if the albedo is known; the reciprocal proposition is equally true: an inaccurate knowledge of A results in an incorrect estimate of H as quantified by Eq. 10a.

Comparison of the approximate solution with Monte Carlo simulations

Selected situations—The validity of the above approximate formulae can be checked by exactly solving the RTE with the same boundary conditions—a vertically homogeneous ocean bounded by a Lambertian reflector at variable depth. Very accurate solutions of the RTE can be achieved, in particular by using Monte Carlo techniques (Mobley et al. 1994). Using such a Monte Carlo code (already described: Morel and Gentili 1991), we have examined various hypothetical and extreme situations as well as a "realistic situation."

For extreme cases, the water is either optically pure, so that scattering originates only from molecules, or conversely, the particle load

Table 1. Input parameters for Monte Carlo simulations with a perfectly reflecting bottom ($A = 1$). The scattering phase function is that of water molecules (M) or particles (P) for the hypothetical cases; for the realistic case both kinds of scattering are involved (M+P); ϖ is either 0.2 or 0.9 for the hypothetical cases and 0.68 for the realistic case; θ_0 is the zenith solar angle. τ_B is the optical depth of the reflecting bottom ($A = 1$), and τ_{max} is the optical depth of a black bottom with $A = 0$. Outputs of the simulations: mean values of the attenuation coefficient (K_d as m^{-1}) computed for the depth interval $(0;\tau_B)$; R_∞ is computed when $A = 0$ at τ_{max}.

ϖ	Type of scattering	$\theta_0 = 0°$		$\theta_0 = 60°$		Overcast sky		τ_B
		R_∞	K_d	R_∞	K_d	R_∞	K_d	
0.2	M	0.0381	0.933	0.0425	1.217	0.0405	1.082	0.5
			0.940		1.222		1.083	1
			0.948		1.225		1.083	2
			0.957		1.223		1.082	4
	P	0.0013	0.806	0.0019	1.062	0.0016	0.940	0.5
			0.812		1.065		0.940	1
			0.813		1.067		0.938	2
			0.818		1.065		0.932	4
								τ_{max} 20
0.9	M	0.4425	0.445	0.4714	0.534	0.4575	0.492	2
			0.472		0.533		0.505	4
			0.495		0.531		0.515	8
			0.510		0.528		0.519	16
	P	0.0570	0.131	0.0814	0.184	0.0700	0.159	2
			0.138		0.190		0.165	4
			0.150		0.197		0.173	8
			0.164		0.196		0.180	16
								τ_{max} 30
				Realistic case				
0.68 (λ = 500 nm)	M + P			$\theta_0 = 45°$ + sky		0.0285	0.0513	1
							0.0521	2
							0.0528	3
							0.0535	5
							0.0540	10
							0.0540	15
							0.0539	20
								τ_{max} 30

is such that molecular scattering becomes totally negligible with respect to particle scattering; in this case, the scattering phase function is that of Petzold (1972) as adopted by Morel and Gentili (1991). These extreme situations are labeled M and P, respectively (Table 1). In addition, the water is either a predominantly absorbing medium or a highly scattering medium; with this aim, the single scattering albedo ϖ is given the value 0.2 or 0.9. Such ϖ values represent limiting values to be observed within the entire visible (400–700 nm) spectral domain in oceanic case 1 waters with various chlorophyll concentrations (*see* figure 2 of Morel and Gentili 1991). For these Monte Carlo simulations, the sky is black and the solar zenith angle (θ_0) is 0° and 60° or the sky is overcast with a cardioidal radiance distribution.

The geometrical depth is replaced by the dimensionless optical depth, defined as $\tau = cZ$, and c (the attenuation coefficient) is given the value 1 m^{-1}. The optical depth corresponding to the bottom depth is denoted τ_B (=cH). For highly absorbing waters ($\varpi = 0.2$), τ_B was given the successive values 0.5, 1, 2, 4 with a reflective bottom of albedo 1; in addition, the bottom was assumed black ($A = 0$) and set at $\tau_B = 20$ to simulate a deep ocean and determine the value of R_∞. For highly scattering waters ($\varpi = 0.9$), τ_B was given the values 2, 4, 8, 16, again with $A = 1$, and then $\tau_B = 30$ with $A = 0$ in order to derive R_∞. With these τ values the behavior of $R(0, H)$ is described between its initial value when the reflector is near the surface and its limiting value (R_∞) when τ_B is large enough so that the bottom influence becomes undetectable. Twelve other situations were also considered with a unique sun angle

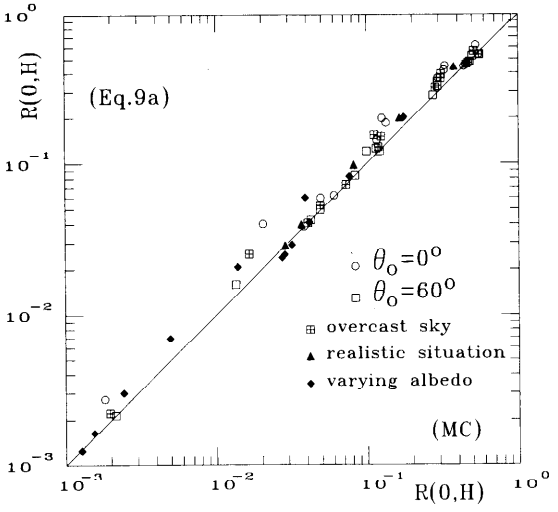

Fig. 1. Reflectance at null depth computed via Eq. 9a (ordinate) or through Monte Carlo simulations (abscissa) in 67 situations described in text (various waters, bottom depths and albedo, sun positions; *see Table 1*). The line represents 1 : 1.

(0°), six bottom albedo values (0.3, 0.1, 0.03, 0.01, 0.003, and 0.001), and two ϖ values (0.2, in this case $\tau_B = 1$, and 0.9, with $\tau_B = 2$).

For the realistic situation, the chlorophyll pigment concentration was set at 0.1 mg m^{-3}. The corresponding optical properties of this water (at $\lambda = 500$ nm) were modeled as by Morel and Gentili (1991), leading to $c = 0.1198$ m^{-1}, $\varpi = 0.68$, and $\eta = 3.5\%$ (η is the ratio of molecular scattering to total scattering). The reflecting bottom was set at $\tau_B = 1, 2, 3, 5, 10, 15$, and 20 with $A = 1$, whereas the deep ocean was simulated with a black bottom at $\tau_B = 30$ ($H = 250$ m, $A = 0$). The sky radiation was accounted for and the Monte Carlo model simulated a coupled ocean-atmosphere system. The barometric pressure was assumed to be 1,013 hPa; vertically integrated water and ozone contents were set at 2 g cm^{-2} and 0.35 cm atm, respectively, and aerosols of maritime type were introduced corresponding to a horizontal visibility of 23 km. The solar zenith angle was fixed at 45°, and the air–water interface was assumed to be flat.

Besides reflectances (including R_∞), the Monte Carlo simulations also produce the values of K_d at any depth. To compare the exact reflectances with the approximate solution given by Eq. 9, we gave the operative diffuse attenuation coefficient, K, the value of K_d (Table 1), computed for the same sun angle and for the same depth interval (from 0 to the depth corresponding to τ_B) but when the bottom (black and at its deepest position) has no effect.

In summary, exact solutions have been obtained (when $A = 1$) for four bottom depths, four types of water, and three illumination conditions and for six other A values, at one τ_B value, two water types, and with the sun at zenith. In addition, the realistic situation includes seven bottom depths ($A = 1$) for one water body and one sun angle. Therefore, for the purpose of testing the approximate solution (Eq. 9) against the exact computation (via Monte Carlo simulations), 67 situations can be compared.

Results of the comparison—An overall view of the comparison between the approximate and exact solutions of the radiative transfer equation in the presence of a reflecting bottom is provided by Fig. 1. For the 67 situations, the reflectances at null depth and for varying bottom depths, $R(0, H)$, as computed through Eq. 9a, are plotted against the corresponding quantities produced by the Monte Carlo code. The agreement between the two categories of results is very good, even though Eq. 9a, as expected, tends to overestimate reflectance values when $(A - R_\infty)$ is positive or underestimate these values when $(A - R_\infty)$ is negative (this situation actually happens for $\varpi = 0.9$ and when A is given values below 0.057; *see Table 1*). The ratio of approximate values to exact values is 1.13 ± 0.19 (SD) and quantifies the importance of the error resulting from the approximations contained in Eq. 9a and from the use of K_d as the unique operational coefficient.

Another way to examine the error is to use the exact reflectance values (obtained from the Monte Carlo simulation) and solve Eq. 9a for K:

$$K = (2H)^{-1} \ln\{[A - R_\infty]/[R(0, H) - R_\infty]\} \quad (11)$$

and then compare the derived K coefficients to the exact (Monte Carlo) K_d values. For particle-dominated scattering (cases P in Table 1), $K : K_d$ ranges between 1.33 ($\varpi = 0.2$, $\theta_0 = 0°$) and 1.01 ($\varpi = 0.9$, $\theta_0 = 60°$). This ratio decreases as ϖ and θ_0 (and hence μ_d) increase and slightly decreases as the bottom deepens, what-

ever the water. For instance for the realistic water, this ratio is equal to 1.145 when τ_B = 1 and 1.067 when τ_B = 5. The above values of the $K:K_d$ ratio would mean that the sum $(K_d + \kappa)$ in Eq. 7 ranges between 2.02 and 2.66 K_d. The latter value is <3.5 K_d reported by Kirk (1989), which was computed in absence of a bottom (only κ_C involved) and for a vertical sun (leading to a minimal K_d value).

The largest discrepancy between approximations and exact reflectances occurs for highly absorbing water ($\varpi = 0.2$) and when scattering is produced by particles. This discrepancy can also be seen in Fig. 2 (cf. figure 1 of Gordon and Brown 1974), where the family of curves in each panel is generated by allowing A to vary in Eq. 9a. When the bottom is deep enough (in terms of optical depth) and whatever its albedo, all curves tend toward the R_∞ value—typical of the water considered. The initial slope and curvature of these curves are reversed when the bottom albedo is either larger or smaller than R_∞.

A more complete comparison can be made by considering the reflectance values not only at null depth but also at various levels inside the water column (Figs. 3, 4). The curves, as produced through Eq. 9b, and the exact results of the Monte Carlo simulations are in extremely close agreement, especially for the realistic situation. The reflectance values, after being multiplied by $E_d(0)\exp(-K_dZ)$, provide the upwelling irradiances, $E_u(Z, H)$; they are compared to exact solutions in Fig. 4.

Even for extreme and somewhat unrealistic cases, the approximation remains efficient, and simple equations such as 9a,b and 10a,b provide a useful tool for predicting reflectances at various depths in the presence of a bottom. With respect to time-consuming Monte Carlo simulations, the advantage of such a simplified approach is to allow the behavior of the reflectance to be predicted in a computationally efficient way and for all wavelengths, provided that the spectral values of the three parameters R_∞, A, and K can be assessed. This predictive capability, based on field determinations of the needed spectral values [$R_\infty(\lambda)$, $A(\lambda)$, and $K_d(\lambda)$], is examined below.

Validation via experimental determinations

Locations, materials, and methods—We used a LiCor LI-1800 UW underwater spectroradiometer (spectral resolution, ~8 nm) to measure spectral downwelling and upwelling irradiances in lagoons near Moorea (a high island, Society Archipelago) and inside the Takapoto atoll (Tuamotu Archipelago). These measurements were carried out in shallow waters with various bottom depths, compositions, and albedos. The selection of the sites rested on the homogeneity of the bottom cover and the proximity to a deep zone, ensuring that R_∞ could be determined in optically similar

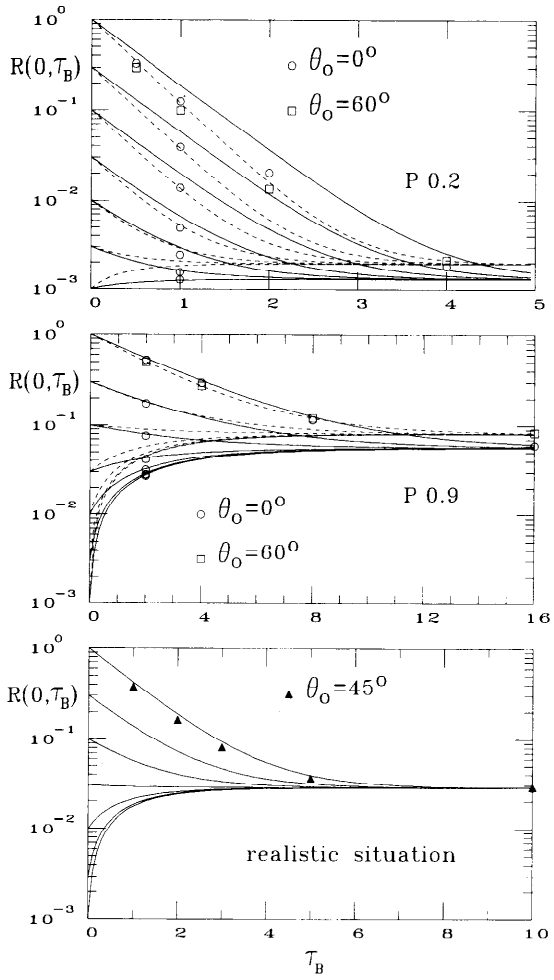

Fig. 2. Reflectance at null depth as function of the optical depth of the reflecting bottom (τ_B) and for various bottom albedos. Each panel is for a particular water type (*see Table 1*). The curves were obtained with Eq. 9a and several values for bottom albedo (A = 1, 0.3, 0.1, . . . , 0.001) and by introducing K_d and R_∞ values obtained via the Monte Carlo code when $\theta_0 = 0°$ (solid curves) or $\theta_0 = 60°$ (dashed curves). The symbols represent the results of Monte Carlo simulations.

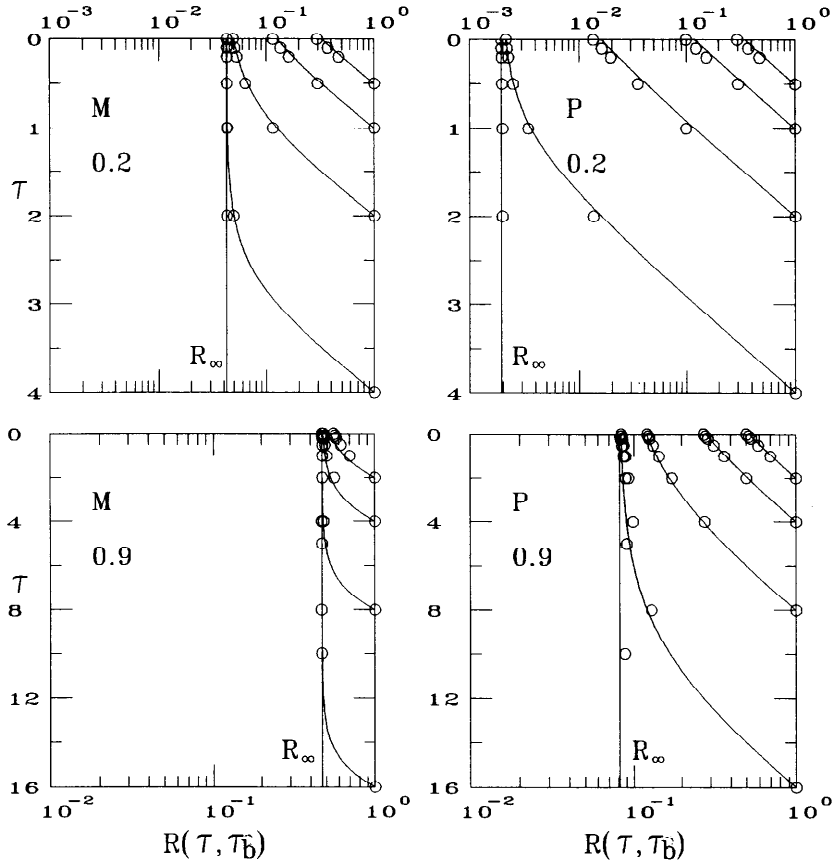

Fig. 3. Reflectances, $R(\tau, \tau_B)$, as function of the optical depth (τ) for various optical depths of the reflecting bottom (τ_B and $A = 1$). Each panel is for a particular water, as indicated (*see Table 1*). The curves are computed by operating Eq. 9b, using K and R_∞ values produced by the Monte Carlo code when $\theta_0 = 60°$; circles represent reflectance values obtained via Monte Carlo simulations, also with $\theta_0 = 60°$.

water. The data were collected during cloud-free days, with calm seas, when solar elevation was high. From measurements of $E_d(\lambda, Z)$ and $E_u(\lambda, Z)$, the spectral values of the reflectance

$$R(\lambda, Z) = E_u(\lambda, Z)/E_d(\lambda, Z)$$

and of the attenuation coefficient for downwelling irradiance, $K_d(\lambda)$, can be derived. The calm sea allowed E_u to be measured a few centimeters under the surface, whereas E_d was measured above the surface and corrected for loss due to reflection (set at 4% regardless of wavelength). These two measurements allow us to compute the reflectance at null depth $R(\lambda, 0)$. The needed $R_\infty(\lambda, 0)$ values were determined in neighboring deep waters ($Z > 40$ m at Takapoto and $Z > 45$–60 m at Moorea). Typical $K_d(\lambda)$ and $R_\infty(\lambda, 0)$ spectra for the deep waters of Takapoto and Moorea lagoons are shown in Fig. 5.

Instrument shadowing prevented the direct measurement of bottom albedo; instead, in vitro reflectance spectra of sampled bottom materials were determined by means of an integrating sphere (LiCor 1800-12) interfaced with the spectroradiometer. Replicate measurements were made for coral sand, two brown algae (*Sargassum* sp. and *Turbinaria* sp.), one green algae (*Boodlea* sp.), and two red encrusting algae (*Porolithon onkodes* and an unidentified one, named *Corallinacea* in Fig. 6). All objects were kept completely wet during measurement. Compacted sand, flat samples of thallus, or encrusted pieces were placed at the port of the integrating sphere. The backscattered signal was recorded in reference to that

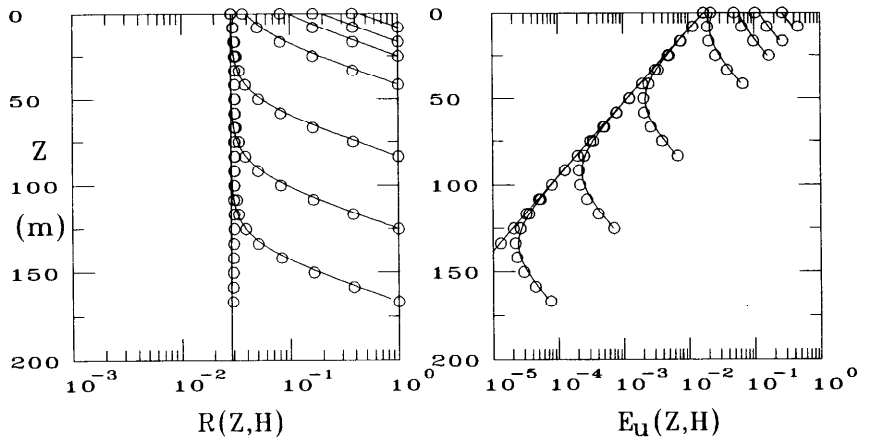

Fig. 4. Left: reflectances as in Fig. 3 but for the realistic situation (note that ordinate is scaled according to the geometrical depths). Right: upwelling irradiances for the same situations as in the left panel, and for an extraterrestrial solar irradiance of 1 W m^{-2} on a surface perpendicular to the sun direction. Circles represent Monte Carlo outputs; curves are obtained with the approximate Eq. 9b.

measured when a $BaSO_4$ diffusing plate replaced the sample. A 2% correction was uniformly subtracted from the measured reflectance to account for the air–water interface reflection. The spectral values of the reflectance by these materials are displayed in Fig. 6.

Results of the validation—Waters are normally very clear and algal biomass is generally low in the coral reef lagoons of French Polynesia, with typical chlorophyll concentrations ranging from 0.1 to 0.3 mg m^{-3} (e.g. Charpy and Charpy-Roubaud 1991; Delesalle and Sournia 1992). In Takapoto atoll, the determination of pigments carried out in parallel with the optical measurements led to an average value of 0.19±0.02 mg m^{-3} (Chl *a* + Pheo *a*). The corresponding $K(\lambda)$ or $R_\infty(\lambda)$ spectra are very close to those of an oceanic case 1 water with the same pigment concentration (Morel 1988), apart from a slightly increased attenuation (and correlated decreasing reflectance) from 450 down to 400 nm (Fig. 5). A similar yet more accentuated departure from case 1 waters is observed for the Moorea lagoon waters (Chl *a* + Pheo *a* concentrations ranging from 0.3 to 0.5 mg m^{-3}). The much larger runoff associated with a high island likely contributes to bring blue-absorbing materials into the lagoon, which enhances attenuation (and depresses reflectance) in the 400–450-nm domain; simultaneously, more scattering particles could slightly raise reflectance values throughout the whole spectrum (*see* Maritorena 1993).

In addition to common features (depressed values below 500 nm and around 675 nm associated with the presence of chlorophyll), the in vitro spectral albedo for macroalgae reflects the specific pigment composition of each taxonomic group (Fig. 6). The green alga (*Boodlea* sp.) exhibits a broad and prominent maximum at 550 nm. The brown algae (*Sargassum* sp.

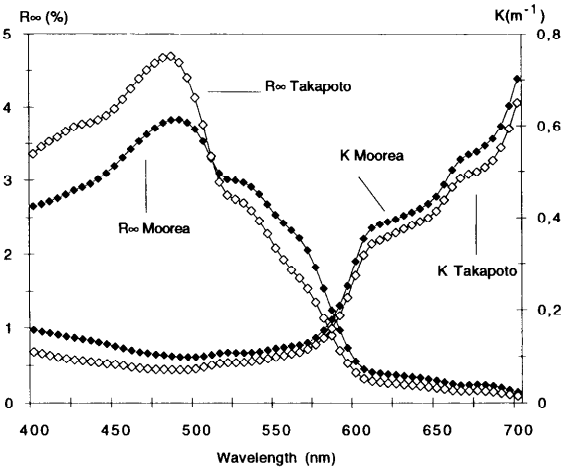

Fig. 5. Reflectance spectra (left ordinate) at null depth when the bottom influence is negligible, and diffuse attenuation coefficient spectra (right ordinate) for deep waters typical of the two islands.

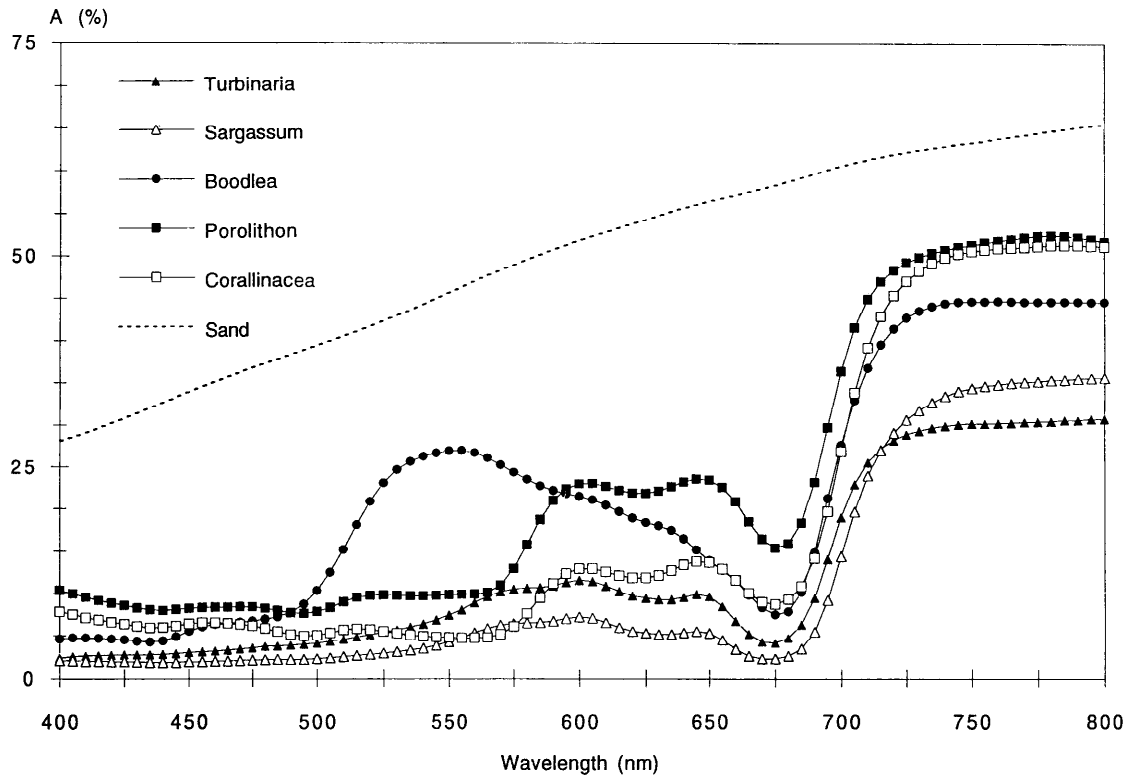

Fig. 6. Spectral values of the albedo for various algae and coral sand.

and *Turbinaria* sp.) albedo remains rather uniformly low throughout the spectrum, with maximum values shifted in the 570–650-nm domain because of strong fucoxanthin (and carotene) absorption. In the green part of the spectrum, the phycobilin pigments depress the albedo values of the two red algae; they have in common a doubly peaked pattern (600 and 650 nm) and, in the blue region, albedo values above those of green and brown algae. The fine coral sand was sampled in emerged zones and is thus free from microphytobenthic organisms, such as cyanobacteria and diatoms, which often colonize these bottoms. The mean albedo of this highly reflective calcium carbonate debris is high, with a smooth ascending slope from short toward long wavelengths.

Some examples of in situ reflectance spectra, as determined just below the surface and above three kinds of bottom, are shown in Fig. 7. Interestingly, in such limpid waters, a sandy bottom even as deep as 15 m has a distinct signature and can produce reflectance values at the surface twice those of R_∞ (*see Fig. 5*). With lower albedos, macroalgae are more elusive though easily detectable, at least in shallow waters, owing to their minimum reflectance in the blue part of the spectrum [where the bottom contrast ($A - R_\infty$) is negative] and to their reflectance maxima (at 550 and 575 nm for green and brown algae, respectively).

The operative $K(\lambda)$ coefficients are given the measured $K_d(\lambda)$ values. Then, by operating Eq. 9a with the relevant $R_\infty(\lambda)$ and $A(\lambda)$ values (from Figs. 5, 6), the reflectance spectra can be reconstructed (also plotted in Fig. 7). The spectral shapes are well reproduced, and a general agreement between the computed and measured values can be seen. For sandy bottoms, the observed reflectances tend to be slightly higher than those derived from Eq. 9a in spite of the overestimation expected from the use of this equation in the case of positive bottom contrast. Silt in suspension is probably more abundant in shallow waters than in deep waters where R_∞ has been determined.

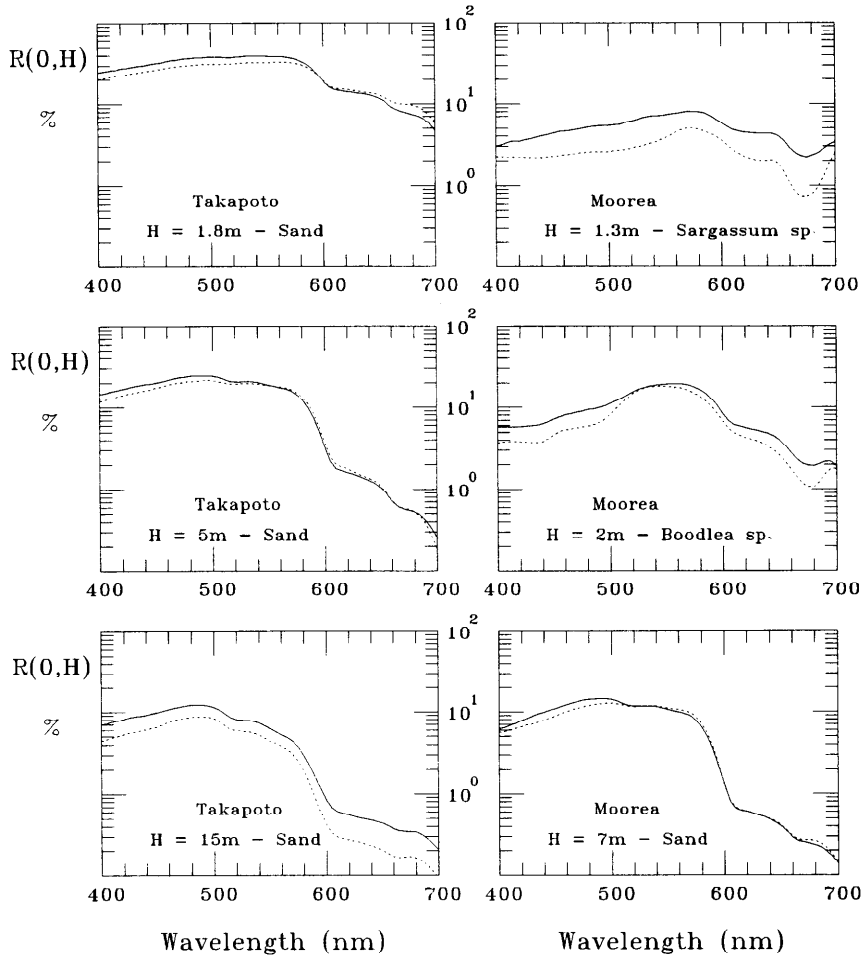

Fig. 7. Measured reflectance spectra (solid lines) and computed spectra (Eq. 9a, dashed lines) at null depth for various locations and bottom conditions.

In contrast, when $(A - R_\infty)$ is negative, an underestimate is expected from the use of Eq. 9a. Such a situation occurs for a bottom covered by brown algae (*Sargassum*) and only within the 400–550-nm spectral range. The slight underestimate of the predicted compared to the measured spectra, however, extends over the full spectral range. This underestimate very likely originates from a contribution of the substratum to the actual reflectance, since perfectly covered bottoms are rarely encountered on the reef. Unfavorable conditions (wave-breaking zone of the outer reef) have prevented reliable measurements from being made above red encrusting algae bottoms. The general agreement between predictions (note that H is not considered an unknown) and the reflectance data is put in evidence by considering all experiments and all wavelengths pooled together and compared to the corresponding computed values (Fig. 8). The spectral reflectances extend from 0.1% (typical of red radiation and deep bottom) up to 40% (blue-green radiation, shallow sandy bottom).

Figure 9A shows the upwelling irradiances at selected wavelengths measured at various levels inside a water column bounded by a sandy bottom at $H = 15$ m. These upwelling irradiances, $E_u(Z, H)$, can be predicted through Eq. 9b by multiplying the reflectances, $R(Z, H)$, by $E_d(0)\exp(-K_dZ)$. At each wavelength,

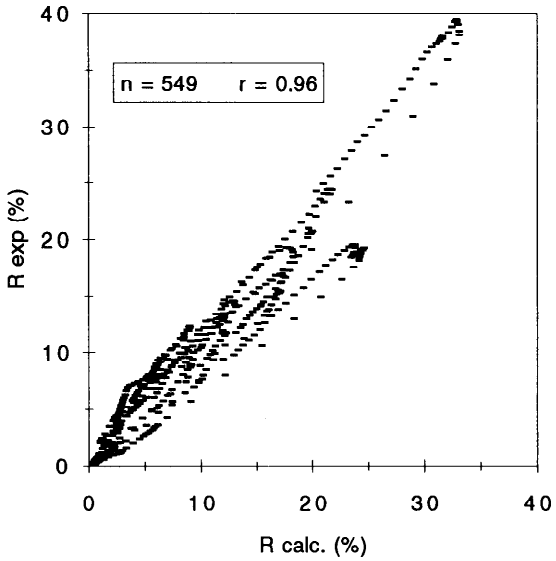

Fig. 8. Spectral reflectance values [sampled every 5 nm within the experimental $R(\lambda)$ spectra] plotted vs. the corresponding values computed with Eq. 9a. All bottom depths and conditions are pooled. The 549 couples lead on average to R_{calc} (%) = 0.93 R_{meas} (%) − 0.13, with $r = 0.96$, and the agreement between R_{calc} and R_{meas} is within ±20% (at 1 σ) except for low values of R (<4%), where it deteriorates.

Eq. 9b is operated with the spectral values of the sand albedo (values shown in Fig. 6) and with the $K_d(\lambda)$ and $R_\infty(\lambda)$ determined in the deep waters of the Takapoto lagoon (Fig. 5). For the less penetrating radiations (red), the upwelling irradiances decrease down to a minimum value and then increase near the floor (*see also* figures 5–8 of Plass and Kattawar 1972), whereas in the blue-green part of the spectrum, the E_u minimum shifts toward the surface and tends to vanish (Fig. 9A), so that a quasi-uniform E_u field prevails between the bottom and the surface.

Predicted and measured values for various wavelengths are in remarkably good agreement, except at 700 nm. An estimate of the inelastic scattering obtained by operating the Monte Carlo code in its transpectral version (*see* Mobley et al. 1994) shows that the Raman contribution (Stavn and Weidemann 1988; Marshall and Smith 1990) can account for the difference. The Raman emission around 700 nm originates from source wavelengths in the 550–570-nm domain. At ~10 m, these green-yellow radiations carry, in terms of scalar irradiance, a flux $\sim 10^5$ times larger than that transported upward by the elastically backscattered red radiations (Fig. 9B). Therefore, the locally emitted nonsolar photons become more abundant (by a factor of 10) than the solar backscattered photons. With a Raman scattering coefficient of 0.003 m^{-1} (a reasonable value for the broad Raman band), the inelastically scattered photons, when added to the elastically scattered photons, account fairly well for the field data.

Discussion and conclusion

In the present problem, it is useless to enter into all the details and complexities of the in-water light field to explain the relatively small differences between the approximate and accurate solutions. Such differences can be put into evidence only when all parameters are perfectly mastered, in particular when Eq. 9 can be operated with the appropriate (i.e. sun-angle dependent) K_d and R_∞ values (Kirk 1984; Gordon 1989; Morel and Gentili 1991). For instance, in a "best" scenario in which there will be no uncertainty in A, R_∞, and K_d, the use of the approximate Eq. 9a still entails an error on the bottom depth estimate; by replacing K by K_d in Eq. 11 and solving for H, it follows that the ratio $H_c : H_a$—computed to the actual depth—is identical to $K : K_d$. Therefore $H_c : H_a$ ranges also from 1.01 to 1.33 for the data shown in Fig. 1. For practical applications and when using Eq. 9 (a or b), mean and supposedly representative values must be selected for K_d and R_∞, leading to uncertainties (in H, if A is known or in A if H is known) at least comparable in magnitude to those mentioned above. In conclusion, the approximate formulae can be safely adopted in operation when interpreting or predicting the reflectance of shallow waters, in particular if R_∞ and K_d have been estimated from remotely sensed data.

There is no straightforward connection between the present approach and the analysis based on photon fates carried out by Gordon and Brown (1974). Their equation 5, which separates the contributions to reflectance from photons that do not strike the bottom from the contributions of those striking the bottom once and twice (when $A = 1$), cannot be simply compared to our Eq. 9a, even if the Monte Carlo simulations of Gordon and Brown and

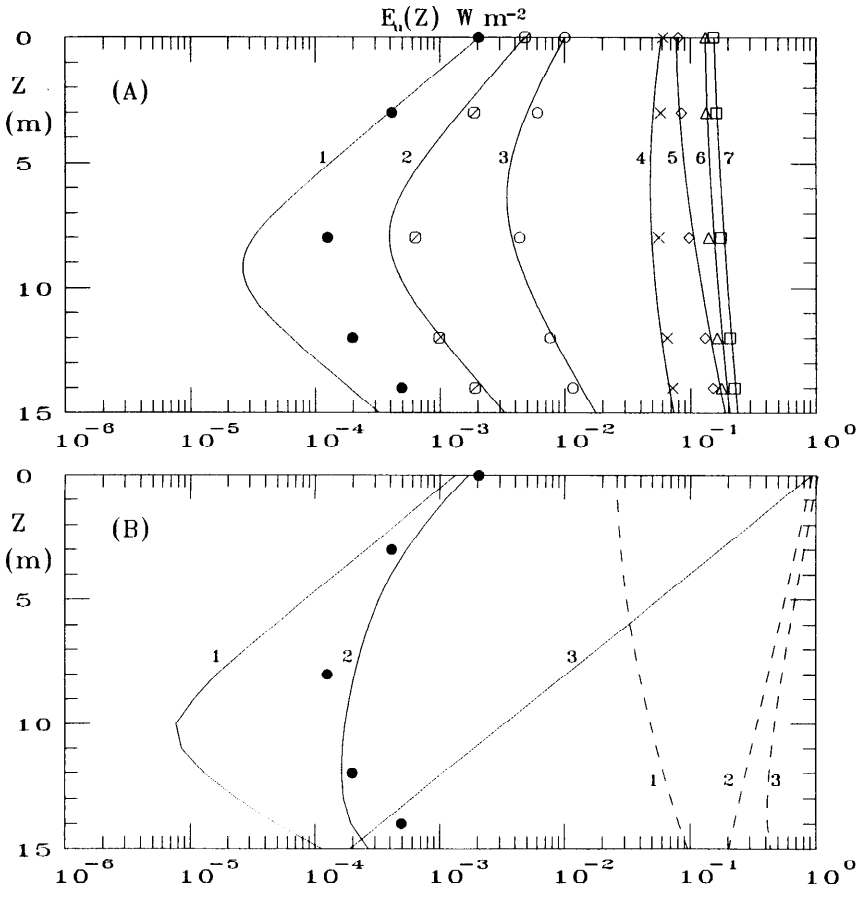

Fig. 9. A. Upwelling irradiances (symbols) at selected wavelengths measured at various levels above a sandy bottom at 15 m in Takapoto atoll (9 June 1988). The curves are computed with Eq. 9b and scaled with the measured irradiance values at null depth. The correspondence between numbers and wavelengths is 1—700 nm, 2—650 nm, 3—600 nm, 4—400 nm, 5—550 nm, 6—450 nm, and 7—500 nm. B. Results of a Monte Carlo simulation accounting for the Raman emission (at 700 nm) from the source wavelength (570 nm) in the presence of a sandy bottom at 15 m (as in panel A). The dashed curves are for 570-nm wavelength and numbered 1—for $E_u(Z)$, 2—for $E_d(Z)$, and 3—for $E_0(Z)$, the scalar irradiance. The solid curves are for $\lambda = 700$ nm, with 1 for $E_u(Z)$ due only to elastically scattered photons, 2 for $E_u(Z)$ when inelastically (Raman) scattered photons are added to those in curves 1 and 3 for $E_d(Z)$. The Monte Carlo simulation has been run with $a(570) = 0.086$ m^{-1} and $b(570) = 0.18$ m^{-1} (leading to $K_d = 0.11$ m^{-1}) and $a(700) = 0.53$ m^{-1} and $b(700) = 0.14$ m^{-1} (leading to $K_d = 0.56$ m^{-1}). Dots represent field data at 700 nm (as in panel A).

those presented here actually agree. Because Eq. 9 is based on measurable properties (R_∞ and K_d) rather than on photon histories (not directly traceable), it is more handy for practical applications.

Although Eq. 9a forms an adequate tool when interpreting the shallow-water reflectance, its use for prediction deserves comment. Equation 9a includes four unknowns; two pertain to the water itself (K, R_∞) and two to the bottom (A and H). Considering a set of equations written for several wavelengths does not improve the situation because new unknowns, apart from H, are introduced. Adding other independent, generally hypothesized relationships between the spectral values of $A(\lambda)$ or between $R_\infty(\lambda)$ values or $K(\lambda)$ values is a way to increase the number of equations when attempting to solve the system. Discussion of these empirical techniques, developed to interpret the radiometric signals (such as those of Landsat-TM or SPOT), is beyond the scope

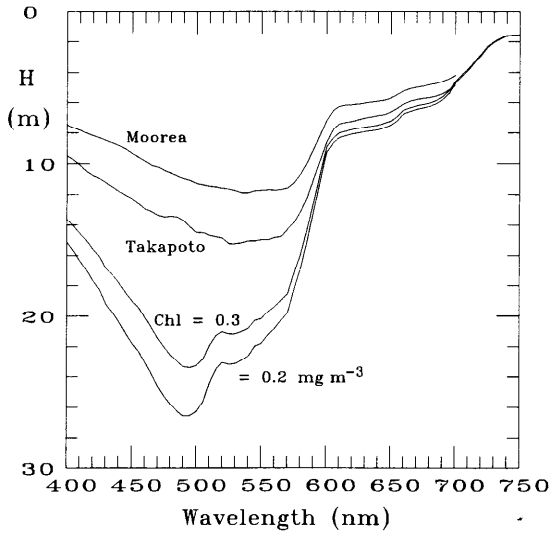

Fig. 10. Depth of a detectable sandy bottom as a function of the wavelength used for its observation from the surface (*see text*) and for several waters.

of our study. However, even if favorable conditions allow the assumption of homogeneous waters (constant K values), it follows from Eq. 9a and 10a that discriminating between albedo patchiness and bathymetric variability remains dubious in the absence of independent in situ information.

The following discussion remains restricted to the easier problem of bathymetry in the presence of coral sand only and to the lagoonal clear waters studied here. The spectral albedo values of this bottom can be, by approximation, linearly expressed as (*see Fig. 6*)

$$A(\lambda) = A(400)[1 + (\lambda - 400)/400].$$

$A(400) = 30\%$; note that $A(\lambda) > R_\infty$ everywhere within the spectrum.

With known values for $K(\lambda)$ and $R_\infty(\lambda)$, Eq. 9a can be solved for H. Assuming, for instance, that an increase in reflectance by a factor of 2, when going from infinitely deep water to shallow water, represents the detectability threshold, the corresponding shallow-water reflectance is then

$$R(0, H) = 2R_\infty,$$

leading to

$$H = (2K)^{-1}\ln[(A - R_\infty)/R_\infty].$$

By reintroducing the spectral dependency of all parameters, the detectable bottom depth depends in a variable manner on the wavelength considered. The "$H(\lambda)$ values" computed throughout the entire spectrum (Fig. 10) apply to the waters of Moorea and Takapoto [$K(\lambda)$ and $R_\infty(\lambda)$ taken from Fig. 5] and also to case 1 waters with chlorophyll concentrations of 0.2 and 0.3 mg m^{-3}, as possibly encountered over the outer reef around the islands [$K(\lambda)$ and $R_\infty(\lambda)$ taken by Morel 1988]. The proviso of a possible detection in case of a doubling in reflectance is not severe for the blue-green part of the spectrum, as R_∞ is already high and its doubling easily perceived. Therefore, accurate measurements at ~500 nm likely would allow the detection of deeper sandy bottoms than suggested by Fig. 10. In contrast, for the red part of the spectrum, the criterion is much more severe, so that R_∞ and its variations are difficult to assess because of their vanishingly low values.

According to their lower albedos (Fig. 6), other bottom covers have a much weaker signature compared to that of sand; therefore, the depth detectable through a reflectance enhancement or lowering (positive or negative contrast) is reduced. Green macroalgae with contrasted spectral reflectivity (depressed values in the blue region and a distinct maximum around 560 nm) would constitute a target more easily identifiable than brown algae, which is practically deprived of any distinct signature in the spectral domain of penetrative radiations (<580 nm). In the near-infrared domain, the albedo similarly increases for all kinds of cover; as a consequence the bottom composition would have a lesser impact on bathymetric assessment. The water absorption, however, severely hinders this possibility, as the detection capability cannot exceed 1 or 2 m even in clear waters.

The need for a high spatial resolution is often emphasized for the study of reef and lagoon systems. The above conclusions, however, suggest that an improved radiometric resolution is also prerequisite for meaningful interpretation of the bottom signature. Spectro-imaging systems, rather than the present broadband sensors, would certainly increase the efficiency of any remote-sensing techniques aimed at the survey of clear coastal environments.

References

ACKLESON, S. G., AND V. KLEMAS. 1986. Two-flow simulation of the natural light field within a canopy of submerged aquatic vegetation. Appl. Opt. **25:** 1129–1136.

CHARPY, L., AND C. J. CHARPY-ROUBAUD. 1991. Particulate organic matter fluxes in a Tuamotu atoll lagoon (French Polynesia). Mar. Ecol. Prog. Ser. **71:** 53–63.

CLARK, R. K., T. H. FAY, AND C. L. WALKER. 1987. Bathymetry calculations with Landsat 4 TM imagery under a generalized ratio assumption. Appl. Opt. **26:** 4036–4038.

DELESALLE, B., AND A. SOURNIA. 1992. Residence time of water and phytoplankton biomass in coral reef lagoons. Cont. Shelf Res. **12:** 939–949.

DUNTLEY, S. Q. 1963. Light in the sea. J. Opt. Soc. Am. **53:** 214–233.

GORDON, H. R. 1989. Dependence of the diffuse reflectance of natural waters on the sun angle. Limnol. Oceanogr. **34:** 1484–1489.

———, AND O. B. BROWN. 1974. Influence of bottom depth and albedo on the diffuse reflectance of a flat homogeneous ocean. Appl. Opt. **13:** 2153–2159.

KIRK, J. T. O. 1984. Dependence of relationship between inherent and apparent optical properties of water on solar altitude. Limnol. Oceanogr. **29:** 350–356.

———. 1989. The upwelling light stream in natural waters. Limnol. Oceanogr. **34:** 1410–1425.

LYZENGA, D. R. 1978. Passive remote sensing techniques for mapping water depth and bottom features. Appl. Opt. **17:** 379–383.

———. 1981. Remote sensing of bottom reflectance and water attenuation parameters in shallow water using aircraft and Landsat data. Int. J. Remote Sensing **2:** 71–82.

MARITORENA, S. 1993. Etude spectroradiométrique de la colonne d'eau et des fonds en milieu lagonaire; implications sur l'imagerie télédétectée à haute résolution dans le visible. Thesis, Univ. Française du Pacifique. 195 p.

MARSHALL, B. R., AND R. C. SMITH. 1990. Raman scattering and in-water ocean optical properties. Appl. Opt. **29:** 71–84.

MOBLEY, C. D., AND OTHERS. 1994. Comparison of numerical models for computing underwater light fields. Appl. Opt. **32:** 7484–7504.

MOREL, A. 1988. Optical modelling of upper ocean in relation to its biogenous matter content (case 1 waters). J. Geophys. Res. **93:** 749–768.

———, AND B. GENTILI. 1991. Diffuse reflectance of oceanic waters: Its dependence on sun angle as influenced by the molecular scattering contribution. Appl. Opt. **30:** 4427–4438.

O'NEILL, N. T., AND J. R. MILLER. 1989. On calibration of passive optical bathymetry through depth soundings. Analysis and treatment of errors resulting from the spatial variation of environmental parameters. Int. J. Remote Sensing **10:** 1481–1501.

PAREDES, J. M., AND R. E. SPERO. 1983. Water depth mapping from passive remote sensing data under a generalized ratio assumption. Appl. Opt. **22:** 1134–1135.

PETZOLD, T. J. 1972. Volume scattering functions for selected natural waters. Scripps Inst. Oceanogr. SIO Ref. 72-78.

PHILPOT, W. D. 1987. Radiative transfer in stratified waters: A single-scattering approximation for irradiance. Appl. Opt. **26:** 4123–4132.

———. 1989. Bathymetric mapping with passive multispectral imagery. Appl. Opt. **28:** 1569–1578.

PLASS, G. N., AND G. W. KATTAWAR. 1972. Monte Carlo calculations of radiative transfer in the Earth's atmosphere-ocean system: 1. Flux in the atmosphere and ocean. J. Phys. Oceanogr. **2:** 139–145.

PREISENDORFER, R. W. 1961. Application of radiative transfer theory to light measurements in the sea. Monogr. Int. Union Geod. Geophys. Paris 10, p. 11–30.

STAVN, R. H., AND A. D. WEIDEMANN. 1988. Optical modeling of clear ocean light fields: Raman scattering effects. Appl. Opt. **27:** 4002–4011.

Submitted: 27 October 1993
Accepted: 23 February 1994
Amended: 26 April 1994